Joint Centre for Mesoscale Meteorology, Reading, UK

Dispersion and removal of pollutants during the passage of an atmospheric frontal system

N. R. Gimson

Internal Report No. 41

December 1994

Met Office Joint Centre for Mesoscale Meteorology Department of Meteorology
University of Reading PO Box 243 Reading RG6 6BB United Kingdom
Tel: +44 (0)118 931 8425 Fax: +44 (0)118 931 8791
www.metoffice.com

Designed and produced by the Met Office © Crown copyright 2001 01/0240 The Met Office logo is a registered trademark.

Dispersion and removal of pollutants during the passage of an atmospheric frontal system

By NEIL R. GIMSON*

University of Reading, UK

SUMMARY

Results are presented from a numerical mesoscale modelling study of the effects of meteorological phenomena on the distribution of contaminants, both airborne and deposited onto the surface, arising from hypothetical idealised release episodes. An Eulerian transport/diffusion/removal model is coupled to the Meteorological Office non-hydrostatic mesoscale model, with removal tuned to represent the wet deposition of pollutants likely to be emitted during a nuclear power station accident.

For a system of fronts which passed over the British Isles on 4 March 1991, the results demonstrate a complex sequence of events in terms of the dispersion and wet removal of pollutants encountering the warm and cold fronts and their associated rainbands, that would not be produced in models with more simplified meteorology, nor in longer range dispersion models which do not resolve the mesoscale well. Significant features found here include the effects of the British Isles orography and local frontogenetic effects on the rainband structure (and hence the washout

patterns), the efficient wet removal of contaminants from the airborne plume (for the scavenging rates chosen here), and the apparent horizontal spread of the plume, produced by a combination of vertical diffusion and vertical wind shear near the fronts.

1. INTRODUCTION

The subject of pollutant dispersion and removal from the atmosphere has, over many years, attracted much scientific attention. Concern over the likely effects on the environment of acid deposition, nuclear war fires, weapons leaks, oil field fires and nuclear power station accidents has motivated this interest. Many groups of scientists in Europe and in the U.S.A. have developed modelling systems for the prediction and subsequent validation of pollution release events. The Chernobyl accident of 1986, for example, provided an opportunity, and also established the requirement, for testing models of transport and deposition of radionuclides on the regional scale (ApSimon and Wilson, 1987; Albergel *et al.*, 1988; Maryon, 1989; Hass *et al.*, 1990; Piedelievre *et al.*, 1990; Bonelli *et al.* 1992). Also, there are studies of "routine" releases from anthropogenic sources, for example in the Eastern U.S. (Saylor *et al.*, 1991), Mount Isa in Australia (McNider *et al.*, 1988), and Florida power stations (Segal *et al.*, 1988). Other, controlled tracer experiments have been carried out to use as test-beds for models. The CAPTEX experiment (Draxler, 1987; Brost *et al.*, 1988b), the Øresund experiment (Gryning, 1985), the Great Dun Fell experiments (Hill *et al.*, 1987; Dore *et al.*, 1990), and releases near the Karlsruhe nuclear research centre (Brusasca *et al.*, 1989), and near the Japanese mountains (Yoshikawa *et al.*, 1990) are some examples.

The transport and removal of air pollution may be modelled in various ways, depending on the length and time scales involved, and on the

relative importance of dynamical meteorology, cloud microphysics, dry and aqueous chemistry. How these aspects are modelled depends on the properties of the pollutant species themselves, that is, whether they are particulate or gaseous, molecular or ionic. The focus of this study is on chemically inert trace metal particles, specifically those micron and sub-micron particles released from, say, a nuclear power station accident, which are light enough to travel far; heavier particles may settle out under gravity near to their source.

For short range dispersion (up to, say, 50 km), Gaussian plume models, under constant meteorological conditions, are suitable (see for example Ku *et al.*, 1987), and these may describe plume rise, advection, diffusion and wet deposition.

To predict the fate of contaminants released into the atmosphere, on timescales longer than a few hours and over distances greater than a few tens of kilometres, mesoscale modelling systems need to be employed. In these the meteorological fields and pollutant dispersion are calculated together prognostically, to give a detailed picture of events over a day or so, over a total scale of several hundred km. The precise domain size and resolution used here are given in section 2.

On the mesoscale, there are several ways of describing the advection of a conserved tracer. Examples are plume trajectory models, and puff trajectory models in which the release is described by a single discrete puff or a number of discrete puffs of material. In these, material is carried along by the winds, spreading laterally and vertically according to some diffusion law. More complex schemes are the Lagrangian "Monte Carlo", or "random-walk", techniques in which the release is considered a stream of particles advected by the model winds and diffused by sub-gridscale turbulence. There are also Eulerian methods where the tracer dynamics are described by an advection/diffusion equation. Carhart *et al.*

(1989) reviewed the performance of examples of all of these types, tested against measurements from a perfluorocarbon release experiment in Oklahoma. Those models which performed best were those with high resolution wind fields, in both space and time. This conclusion had also been reached by Kuo *et al.* (1985) and Draxler (1987). Saylor *et al.* (1991) extended this requirement to include high resolution precipitation data.

In this study an Eulerian framework is used. Such methods have in the past suffered the effects of numerical diffusion (which Lagrangian methods do not), but modern computational schemes have largely alleviated this. Also, it is usually more straightforward to deal with physical or chemical processes such as removal and reaction kinetics in Eulerian models. One criticism though, is that scales of motion of the pollutant may be smaller than the scales resolvable by the meteorological model grid. This is especially true in the early stages of a release near to the source: a mesoscale grid length of, say, 15 km can only resolve scales of 60km or more without serious computational dispersion problems. This aspect will be addressed in a later paper.

Concerning the diffusion of a tracer, there are again a number of ways of describing the spread of a cloud of contaminant due to turbulent motion. For Gaussian puff or plume models, it is common to derive a measure of the lateral and vertical spread in terms of the distance travelled downwind and the Pasquill stability class defined by the wind speed and stratification. Eulerian models may use diffusion coefficients, derived using simplified equations for second-order turbulent fluxes. In the following, the only prognostic equation in second-order quantities is for the turbulent kinetic energy (*TKE*); tendencies of other fluxes are omitted. This is in essence the $1\frac{1}{2}$ order closure used by Yamada and Mellor (1979) (termed "level 2.5 model" in their paper). Usually, due to the disparity in scales between the horizontal and vertical grids in

meso-α-scale models (where the horizontal grid spacing is of the order of a few kilometres) the diffusion is applied only in the vertical, though this can, through the effects of vertical velocity shear in the planetary boundary layer lead to the horizontal spread of contaminants, as found by McNider *et al.* (1988), for example.

Modelling washout and deposition to the surface has also attracted much attention, as this is the first stage of a pathway to human contamination. Detailed microphysical models, in which the evolution of the cloud drop size spectrum, precipitation size spectrum, particle size spectrum, and their mutual interactions in the nucleation and condensation processes have been developed by Flossman and co-workers (Flossman and Pruppacher, 1988; Alheit *et al.*, 1990; Flossman, 1991). These have thus far been used mainly with idealised meteorological situations, for instance, one-dimensional or two-dimensional convective clouds. For larger scale, more complex meteorological situations parameterizations are used which effectively average over the size spectra and formulate the problem in terms of "bulk" concentrations of pollutants, and of total rain and snowfall rates. The mathematical treatment of this is frequently based on the work of Slinn (1979, 1984), though more recently there is a tendency to account for microphysical processes such as evaporation and accretion, basing them on prescribed particle and drop size distributions (Tsai, 1987; Nickerson *et al.*, 1986; Berkowitz *et al.*, 1989; Chaumerliac *et al.*, 1990). This study is mainly concerned with the meteorological effects on contaminants, and the treatment of removal will be fairly simplified.

The presence of mesoscale weather phenomena, such as fronts and convective clouds, can, due to complex wind, turbulence and precipitation patterns, have an important bearing on the fate of a plume of contaminants. These features are not incorporated into Gaussian plume models, nor are they captured fully by regional or global models, in which

mesoscale features are not well resolved. The same may be said of mesoscale models with few levels in the vertical, or dispersion models which do not update the meteorology very frequently. This study uses a model which has high temporal and spatial resolution in three dimensions for both the meteorology and the pollutant dispersion. The aim of the study is therefore rather specific; to investigate the effect of the passage of an active midlatitude frontal system on the distribution of trace contaminants from idealised releases. This problem has not been addressed, although there exist other modelling systems capable of doing so. Most notable is that of Pielke and co-workers at Colorado State University (Segal *et al.*, 1988; McNider *et al.*, 1988). Nitrogen and sulphur chemistry in warm and cold fronts has been considered by Hegg *et al.* (1984, 1986) and Rutledge *et al.* (1986). Their focus was on the frontal precipitation mechanism, and the chemical reactions in the rainbands. Their front was stationary and two dimensional: here, evolving meteorological conditions are considered, which include a propagating frontal system.

This study will attempt to establish a methodology whereby an actual pollutant release can be modelled. Treating idealised releases means that these predictions cannot be verified against observed data; however it does allow a general understanding of the mesoscale dispersion to be gained. The novel features here include the use of a predicted evolving *TKE* to determine diffusion, state-of-the-art schemes for advection of the pollutants, and description of pollutant variations in the horizontal in the range 15 km to 1000 km and in the vertical in the range 100m to 10 km. The aim is to understand the factors, and their relative importance, making up the mesoscale pollutant dispersion. This is as important as simulating an actual case.

Section 2 describes the models used. Section 3 illustrates the

observed synoptic situation and the mesoscale forecast of the frontal system over the British Isles. Section 4 describes some contaminant release runs. The work is discussed and summarised in section 5.

2. THE METEOROLOGICAL AND CONTAMINANT MODELS

The meteorological model used is the United Kingdom Meteorological Office (UKMO) mesoscale forecasting model, based on the non-hydrostatic model of Tapp and White (1976), which was operational until December 1992. There are 89×91 15km grid points in the horizontal and 32 levels in the vertical, from 1.25m to 14025m above the surface. The timestep usually employed is 60 seconds and the domain area covers the British Isles, part of France and the southern tip of Norway. An account of the physical parameterizations and its coupling with other UKMO models and observing systems is given by Golding (1990) and Wright and Golding (1990); only those features particularly relevant to pollution modelling are mentioned in this section.

Firstly, the high spatial and temporal resolution of the meteorological fields are, as pointed out by Saylor *et al.* (1991), crucial to the accurate transport of contaminants. Advantages are also gained by "nudging" the evolving fields towards observational data (Kao and Yamada, 1988). The non-hydrostatic model boundaries are updated using Unified Model forecast data, guiding the mesoscale forecast by synoptic-scale changes. In the boundary layer, the vertical resolution is high, with fifteen levels in the lowest kilometre. Secondly, the 1 1/2 order turbulence closure (based on Yamada and Mellor, 1979) in the mesoscale model may be used for tracer diffusion. Brost *et al.* (1988a) compared various advection schemes and diffusion parameterizations, in their regional Eulerian model, and found greater sensitivity to the type of diffusion than to the advection scheme. The UKMO model diffusion

coefficients for heat and momentum are expressed in terms of the predicted *TKE*, vertical shear, static stability and several empirically determined eddy correlation timescales. Thus the amount of vertical diffusion is stability dependent. This represents a comprehensive turbulent diffusion scheme designed to give a full description of the boundary layer. Here, this scheme is also applied to the vertical spread of contaminants.

The amount of cloud water/ice and gridscale precipitation is diagnosed every timestep, using microphysical schemes designed to realistically model condensation, evaporation, melting, freezing, autoconversion and accretion rates of vapour, cloud water, rain, snow and ice, and the scavenging of airborne contaminants by collision with hydrometeors is dependent on these diagnosed quantities. The warm-rain scheme is based on the seeder-feeder mechanism (Rutledge and Hobbs, 1983), where rainfall from an elevated region, the seeder cloud, is enhanced as it falls through the feeder cloud at lower levels. An account of the consequences of this process for deposition in complex terrain is given by Dore *et al.* (1990), and will be discussed later in the light of results from section 4. Washout due to inertial effects such as collision and coalescence between drops and particles is parameterized in terms of precipitation amounts. The nucleation of cloud droplets and ice crystals requires the presence of contaminant particles which act as condensation nuclei, and the eventual precipitation distribution should depend on the properties of these particles. This is not directly accounted for here; it is assumed that the tracers to be modelled are not a significant contribution to the total atmospheric aerosol and that their presence does not affect the nucleation and condensation rates determined by the mesoscale model.

It is feasible that the model described below could, if coupled with a sub-model for the near-source plume be used as a predictive tool in the

event of an accidental release. Yoshikawa *et al.* (1990) developed such a model for nuclear releases in Japan, though as yet precipitation scavenging is not included. A successful prediction of the consequences of an accidental release depends crucially on the initial source specification. This is rarely known until after the event, thus a more realistic requirement of such a system would be, for example, to locate surface contamination in a cumulative sense soon afterwards.

The pollutant concentration χ obeys an advection/diffusion equation, written in flux form as

$$\frac{\partial \chi}{\partial t} + \nabla.(\underset{\sim}{u}\chi) = \mathcal{S}_e + \mathcal{S}_d + \mathcal{S}_w, \qquad (1)$$

where the sources on the right hand side of the equation are due to the emission, diffusion and washout of pollutants respectively. The unit of concentration is the Becquerel per metre cubed (Bqm^{-3}), where the Becquerel is a unit of radioactivity representing 1 disintegration per second. The finite difference grid is the same as that for the meteorology, and the contaminant is advected with the full three-dimensional velocity $\underset{\sim}{u}$, the mesoscale wind field. Grid point values of χ are at the same locations as potential temperature in the meteorological model, and ∇ represents the three-dimensional gradient operator in x,y,η-coordinates, where the vertical coordinate η is the height above the surface. The numerical advection scheme is total variance diminishing (TVD), which eliminates the spurious oscillations that occur in high order schemes, particularly at discontinuities. This is achieved by adding to the first-order fluxes of χ a limited amount of "anti-diffusive" flux, but still allowing the scheme to be high order where possible. In the zonal direction, at the ith grid element boundary, the flux is written in finite difference form as

$$(u\chi)_i = F_i^{(l)} + \phi_i(F_i^{(h)} - F_i^{(l)}), \qquad (2)$$

where $F_i^{(l)}$ and $F_i^{(h)}$ are the low and high order finite-difference

approximations to the fluxes, respectively. The method of finding the limiter ϕ_i, which depends on χ, closely follows that of Sweby (1984), such that it is as near to unity as possible, whilst still maintaining the TVD property. $F_i^{(l)}$ is a first order upwind representation of the flux and $F_i^{(h)}$ is fourth-order centred in the horizontal and first-order centred in the vertical (or second-order on a regular vertical grid). The resulting scheme is free of computational dispersion, is of high order away from discontinuities and χ remains non-negative. The advective fluxes for each direction are applied successively, as at present no suitable multidimensional scheme exists.

Vertical dispersion of χ, due to sub-grid-scale turbulence is expressed as

$$\mathcal{P}_d = - \frac{\partial \tau}{\partial \eta}, \tag{3}$$

where τ is the subgrid-scale vertical flux of χ.

In the mesoscale model, flux-gradient relationships are derived for heat and momentum, following the $1\frac{1}{2}$ order model of Yamada and Mellor (1979), leading to diffusion coefficients as functions of bulk quantities. Here the thermal diffusivity K_h is also used for χ, whence

$$\tau = - K_h \frac{\partial \chi}{\partial \eta}. \tag{4}$$

At the lowest level, a dry deposition velocity v_d is defined, such that

$$\tau_0 = - v_d \chi_{1.25m} \tag{5}$$

A value of 0.3 cms^{-1} is chosen for v_d, typical of fine particulate material; that reaching the lowest model level diffuses slowly to the surface.

The rate of scavenging of contaminant by falling hydrometeors, due to diffusion, interception or impaction processes depends in a complex way on the particle size, drop size, drop fall speeds and collection efficiency,

as discussed by Slinn (1984). Here, the situation is simplified by writing

$$\mathcal{S}_w = - \Lambda \chi, \tag{6}$$

and, under certain assumptions about size spectra, fall speeds and efficiencies, Scott (1982) has shown theoretically that

$$\Lambda = a_r P_r \hat{}(b_r) + a_s P_s \hat{}(b_s), \tag{7}$$

where P is the precipitation rate, and subscripts r and s refer to rain and snow respectively. Jylhä (1991) calculated values of the constants a_r, a_s, b_r and b_s from observations of material from the Chernobyl plume over Finland. The values are averages over many days, many locations and many weather types. Also, condensation and freezing nucleation, and resuspension through evaporation are effects presumed included in (7). Jylhä found $a_r = a_s = 10^{-4}$, $b_r = 0.64$, and $b_s = 1.2$, such that if P is in mmh^{-1}, then Λ is in s^{-1}. These were derived using only the surface precipitation field, assuming uniformity with height. Here, however, the three dimensional precipitation fields are available, and the removal scheme may be improved upon by requiring that the surface deposition is calculated as if the precipitation rates were uniform with height. To do this, we introduce a factor $\mathcal{F}$, whence

$$\Lambda = \mathcal{F} \, (a_r P_r \hat{}(b_r) + a_s P_s \hat{}(b_s)). \tag{8}$$

The deposition rate is then

$$\dot{\mathcal{D}}_w = \mathcal{F} \int_0^{14025} (a_r P_r(\eta)^{br} + a_s P_s(\eta)^{bs}) \, \chi(x, y, \eta) \, d\eta. \tag{9}$$

Consistent with observations, it is necessary for

$$\dot{\mathcal{D}}_w = (a_r P_r(0)^{br} + a_s P_s(0)^{bs}) \int_0^{14025} \chi(x, y, \eta) \, d\eta. \tag{10}$$

Elimination of $\dot{\mathcal{D}}_w$ between Eqs. (9) and (10) gives $\mathcal{F}$, which will depend on x and y but not η. This parameterization leads to a decrease in deposition if rain evaporates before reaching the ground; if snow melts to rain as it

descends, the contaminant it carries is still deposited. These effects are not in Eq. (7). (Eq. (8) does not account for partial cloud cover, where the precipitation rate applies to only part of the grid volume. To incorporate this, Eq. (7) should be modified, but unless the cloud cover is small, they will make little difference).

$\mathcal{S}_e$ describes a continuous release from a particular location. The advection scheme used is robust enough to deal with a point source, and simple numerical tests have shown the scheme to be free from computational dispersion. However, one grid point in a model actually represents a whole grid volume, and a physical source is, in reality, sub-gridscale. Ideally, the initial growth of a plume should be described by a sub-model, and transposed to the mesoscale grid when it is large enough. For the idealized runs here, however, a continuous source is included, spread over several grid volumes.

3. SYNOPTIC FEATURES AND MESOSCALE FORECAST

a) Synoptic situation.

The case considered is the frontal system associated with the depression which approached the British Isles between the 4th and 5th of March 1991. The surface pressure analysis and positions of fronts are shown in Fig. 1 for 1800 GMT on 4 March 1991. A low pressure centre was situated at about 15°W, remaining at that longitude for twenty-four hours while deepening to 978mbar. It tracked slowly northwards, as a secondary to a more intense low, with central pressure 964mbar, at 53°N, 37°W. Hence the geostrophic part of the near-surface flow was, on the whole, southerly during this period. The frontal system associated with the secondary low possessed an eastward component, sweeping the cold front across the British Isles as the occlusion took place, while the warm front travelled northwards.

At midday on the 4th a broad swathe of cloud, as wide as the British Isles, occupied the warm sector, bounded on its western flank by the cold front, and extending south to Spain. The mesoscale forecast indicates that this cloud band extended up to about 9 km, with a cloud base height about 1.5 km. Hence most of the United Kingdom had no sunshine on the 4th. To the west of this cloud band - behind the cold front and in the vicinity of the low centre - the cloud was patchier, and in some places much shallower. Twenty-four hours later, this region had moved north eastwards and occupied the northern half of the British Isles, the main cloud band now being over the North Sea. Cloud previously far south, over Spain, now covered central and southern England, producing up to 5mm of rainfall during the day of 5 Mar.

b) Mesoscale forecast.

The mesoscale model operational forecast starting at 1200 GMT 4 March 1991 is repeated for this study. The initial fields for the 18 hour forecast were calculated using the interactive mesoscale initialization (IMI) procedure (Wright and Golding, 1990), and lateral and upper boundary updates are from the UKMO Fine Mesh model. The case presented here is identical to the original forecast, except that due to computational storage restrictions the horizontal extent of the domain is decreased from 88×91 to 65×65 points, excluding Norway and the Atlantic to the west of Ireland from the domain. For the sake of compactness of this paper, only a limited selection of the forecast fields will be presented. These are for 1200 to 2300 GMT for 4 March and midnight to 0600 GMT for 5 March 1991.

From now on, unless η is mentioned explicitly, heights will be above sea level, and the cartesian co-ordinate z will be used. Some fields are shown for 1500 GMT at various levels in Fig. 2. Equivalent potential temperature (θ_e) is plotted to indicate the positions of the fronts at

these levels. At z = 1500m (Fig. 2(b)) the warm front is especially clear, oriented NW-SE with θ_e gradient up to 10K per 100km. The cold front is mainly distinguishable near the southern boundary, with similar θ_e gradients. Total precipitation rates (the sum of rain and snow rates) are shaded if greater than 1 mmh^{-1}, and the band is mainly parallel to the occluded front in the north and the cold front, with small patches at the warm front. Orographic enhancement of the precipitation rate leads to some higher rates (above 5 mmh^{-1}) in the cold frontal band above Wales. The horizontal wind is, south of the warm front and occlusion, approximately southerly, with a speed of about 31ms^{-1} in the west of the domain. In the north, the wind is south-easterly, and strongest over Scotland, the change in direction arising through the presence of the active front. At the 500m level (Fig. 2(c)) the fronts and rainbands are in similar locations and have similar strengths to those at 1500m, although the closer proximity of the surface leads to small-scale distortions of the θ_e-field due to orography and land/sea contrasts. Winds are generally weaker (about 20ms^{-1}) and it is notable that the south-easterlies are over much of central England and Wales, in the warm sector. At z = 3500m (Fig. 2(a)), the warm front is much less well defined, and is situated further north than at lower levels. The cold front is more distinguishable, extending about 500km in from the southern boundary. The precipitation band is situated as at the other levels, but the (snow) rates are lower. The wind speed is also similar to that at 1500m, although its direction is different throughout most of the domain.

The system progresses north eastwards, and the fields at 2100 GMT are shown in Fig. 3. The winds at both 1500m and 3500m both now have westerly components, while at 500m the flow is more southerly. The shear across the warm front is still evident at 1500m but at 3500m this front is no longer in the domain. The structure of the cold frontal precipitation is notable

in that it is now in two main sections (at all three levels). The precipitation rates are as high as they were six hours previously, when they were enhanced over the orography of Wales and northern England. Between 1500 and 2100 GMT they have decreased and increased again. Inspection of the horizontal deformation, in relation to the direction of the θ_e-gradients reveals that over central England and off the North East England/South East Scotland coast, frontogenetic forcing is associated with ascent, condensation and precipitation. This localised forcing is significant between 1900 and 2300 GMT at 1500m and 500m. At 3500m (Fig. 3(a)), the forcing is much weaker and not coincident with the precipitation band, as the cold front slopes with height. Also, as a result of the forcing, the θ_e-gradient has increased at both 1500m and 500m (Figs. 3(b) and 3(c)), to the east of the northern portion of the rain/snowband. Behind the main precipitation bands are other more localised patches of rain, travelling north-northeastwards.

Towards the end of the forecast, the frontal system approaches the boundaries of the domain, leaving behind a smoothly cyclonic wind field, relatively free of small scale features, at all levels (Fig. 4). The precipitation in the main band is less intense, although it is spread over a larger area than at 2100 GMT the previous evening. Behind the cold front, there are small areas of precipitation located, at 1500m and 500m (Fig. 4(b,c)) on the upstream slopes of both the north of England orography and the Scottish Highlands. The clouds do extend up to 3500m but no snow is present at this time. This precipitation is associated with the secondary cloudy region originally in the west of the domain. Although the flow over the orography is at about $20ms^{-1}$, the precipitation bands approach from the south-west and remain, through local effects, at the same location until about 0500h.

It is not informative to show horizontal sections of *TKE* or diffusion

coefficients, as the fields contain much small-scale variation. However, a general idea, albeit extremely brief, of values of K_h is required, to explain, or predict vertical contaminant spread through turbulence. As might be expected in cloudy regions, diffusion is large, with K_h = O(10^3 m^2s^{-1}) and *TKE* = O(1 m^2s^{-2}) above the cloud base level, correlated with vertical velocity where it is positive. Away from cloudy regions, or if the cloud base is high, K_h = O(10^{-3} m^2s^{-1}). Values in the boundary layer are intermediate, about 10 m^2s^{-1}, whether cloud is present above or not.

4. POLLUTANT DISTRIBUTIONS

The discussion of the meteorological evolution is focused on those features important to the transport of contaminants: the wind field for advection, *TKE* and thermal diffusion coefficients for vertical dispersion, and the precipitation fields for washout. To examine the relative importance of these features to plumes with sources at different locations and with different effective heights, integrations are carried out, with the contaminant source at various positions relative to the frontal system. The following contains descriptions of results from these integrations, using the meteorological data from 4 March 1991. Table 1 outlines the characteristics of the release and the variant of the contaminant model used for each integration.

An estimate of the total release of Caesium-137 from the Chernobyl accident is 3.7×10^{16} Bq over the 10 days after 26 April 1986 (Piedelievre *et al.*, 1990). To produce values of a similar order of magnitude, the modelled contaminant is emitted at a constant rate of 4×10^{10} Bqs^{-1} from a localised source, which is ellipsoidal in space, with radius 60km and depth 800m, and a maximum point value of the emission rate at its centre of 0.029 $Bqm^{-3}s^{-1}$. This is the same for each run. These dimensions are rather large, chosen to give a fairly widely spread pollutant

distribution, to demonstrate more clearly the effects of meteorological phenomena. The primary interest here is in the consequences of the frontal system for plume dispersion and not necessarily in a perfectly realistic source description.

(a) Runs A to E.

Results from these runs are presented together for intercomparison, since the source is centred at the same location in each, (x, y) = (400km, 150km).

(i) Horizontal motion of the plume.

A general picture of the transport of most of the plume material in Runs A and B can be obtained by consideration of its evolution in Run A at z = 1.5km, as the source level for these runs is η = 1.5km. Initially the warm sector is over the source region, and the amount of contaminant at this level does not increase significantly, despite the constant emission rate. It is lifted during the first 6 hours. At 1800h, the cold front passes over the source, and from this time onwards significant amounts of contaminant can be seen at z = 1500m (Fig. 5(a); note that for clarity the source centre is plotted on Fig. 6(a)). The plume at this level starts to extend north-northeastward, advected with the velocity field behind the cold front. As the frontal system progresses, the winds change direction such that the main part of the plume is swept laterally, from NW to SE, across England between midnight and 0600 GMT (Fig. 5(b,c)), and the part furthest from the source at this level advances along the cold front (which is itself moving) towards the strong southerlies in the north. There this part begins to be sheared laterally from the rest of the plume. By the end of the forecast period, much of the plume is aligned parallel to the cold front. A very similar evolution occurs at this level in Run B, but with somewhat lower magnitudes of χ.

(ii) Vertical spread of contaminants by advection.

In the warm sector, there are several mechanisms by which pollutants may be carried to new levels; through advection by the resolved vertical winds, which may contain small-scale bands of ascent and descent; through turbulent diffusion, which in this cloudy region is appreciable up to about 9km, or through removal in which contaminants are washed out by precipitation and deposited directly onto the surface.

In the first few hours, several bands of ascent pass over the source, and the pattern of contaminant at z=3500m for Run A (with $\mathcal{S}_w=\mathcal{S}_d=0$) bears this out. By 1800 GMT the contaminant is contained in a north-south oriented band with several local maxima in activity (Fig. 6(a)). This is due to the plume encountering the various ascent and descent regions of the warm sector which are themselves superposed on a general uplift in this sector. Viewing the whole plume sideways on (Fig. 6(b)), it is seen that the material at z = 3500m is at different levels relative to the upper and lower plume boundaries. The shape of the contaminant distribution in Fig. 6(b) is not simply due to flow over the orography, as the northern end of the plume has risen several kilometres. Later, the activity decreases at this level and some material passes through the northern boundary. When diffusion and removal are included (Run B), much less material reaches z = 3.5km; values are never greater than 4.6 Bqm^{-3} (whereas they reach 18.9 Bqm^{-3} in Run A), and they extend over a smaller area.

(iii) Vertical diffusion of contaminants.

To reach levels below the source, contaminants may descend with the resolved velocities or diffuse downwards due to turbulence. Material first appears at 500m in Run A after 12 hours, below the the leading edge of the z = 1.5km plume, just behind the cold front. The plume is in the post-cold frontal descent region for many hours before noticeable quantities arrive

at 500m, as vertical velocities are only a few cms^{-1}. The plume reaches a peak concentration of only 11.9 Bqm^{-3} at 0600h, shown in Fig. 7(a). Again, there are small scale maxima in activity. However, material may *diffuse* downwards much earlier, as shown by Run B, in which the diffusion and removal terms of Equation (1) are nonzero. By 2100 GMT there is a peak value of 6.8 Bqm^{-3} in the plume which has diffused downwards and advected northwards (Fig. 7(b)). At 0300 GMT the low level plume extends from the source, over the northeast coast of England. It is wider at its northern end where the peak activity is 12.0 Bqm^{-3}, and this apparent spreading (Fig. 7(c)) is not due to horizontal diffusion - there is none in Equation (1). In fact, it is due to the combined effects of vertical diffusion and horizontal advection. Material diffuses downwards while the plume at higher levels is being swept sideways. It is also transported vertically, in the post-cold frontal descent. For comparison with Run A, χ at 500m in Run B is shown in Fig. 7(d).

(iv) Removal by scavenging and deposition.

A major motivation for the study of air pollution is a need to assess the likely effects of contamination on man. Common pathways to human contamination are through radioactivity from deposited material penetrating clothes (γ-radiation emitters) or through the consumption of material that has contaminated crops or livestock. (α-particles, on the other hand, are stopped by clothing, but may still be inhaled). The nucleation of particles and their collection to form raindrops acts to concentrate pollutants into a small volume (the raindrop volume), which falls towards the surface. This wet deposition mechanism turns out to dominate over dry deposition in the runs described here, but this is situation dependent, as in the absence of clouds and precipitation and with a low level source, dry deposition would be the only removal process.

At the start of these integrations the source is in the cloud band in the warm sector. Precipitation therein removes most material in the first 6 hours, before the cold front passes completely over the source region. The accumulated deposition for the first 9 hours of Run B is shown in Fig. 8(a). The peak value of 78.9 $kBqm^{-2}$ over the orography of Wales is a signature of the orographic enhancement of precipitation leading to a high scavenging rate, and there is always fresh material emitted which can be washed out in that location while the rainband is present. The band of deposition with values greater than 1 $kBqm^{-2}$ (contour not plotted) extends to the far north east of England. This rapid removal restricts the ascent of material, hence the difference in amounts at 3.5km between runs A and B. The total deposition changes little after 1800h.

To produce a reliable prediction of the fate of contaminants released from a local source, there must be an accurate specification of the source. It is shown here that different vertical distributions of the source can alter the patterns of eventual transport and deposition, due, in frontal systems, to vertical wind shear, narrow bands of ascent and descent and the structure of the precipitation bands. The effective height at which the pollutants are injected into the atmosphere may not necessarily be the top of the stack from which material is emitted. There are often plume rise effects, as a hot plume is buoyant relative to its surroundings, or the plume may have a large vertical momentum, if it is the result of an explosion.

In Run C, the source is centred at η = 500m. The airborne plume progresses northwards in a qualitatively similar way to its Run B counterpart; it is the deposition pattern that is of most interest. At 2100h, the accumulated deposition pattern (Fig. 8(c)) is similar to Run B, except that it does not stretch as far north, and is somewhat wider. The two plumes encounter different horizontal velocity fields, as they are at

different levels. The deposition patterns for Runs B and C diverge further at later times. During the final 6 hours there is little removal in Run B (Fig. 8(b)). During this period, the cloudy region behind the cold front passes over the UK, with associated precipitation confined largely to the lowest 3 km. Precipitation rates rarely exceed 1 mmh^{-1}, except over the North of England and in Scotland, on upstream orographic slopes. Correspondingly there is deposition in Run C in these locations (Fig. 8(d)), up to 20.0 $kBqm^{-2}$, compared with 77.5 $kBqm^{-2}$ in the first 9 hours. In this run, most of the contaminant material is at low levels, where winds are southerly, advecting the plume over the whole of the North of England, and the Eastern half of Scotland, whereas in Run B the bulk of the plume is 1 km higher where the winds have a westerly component. In that case the plume misses the northwest of England and all of Scotland. Comparing the volume integrated activity between Runs B and C (Fig. 9), rapid removal occurs between 1400 and 1800 GMT in both runs, where, integrated over the domain, $|\mathcal{S}_w|$ is greater than $|\mathcal{S}_e|$. Later, after 0200h, differences are, as a proportion of the total plume, small. However, there are large differences in surface contamination locally, as a consequence of a different vertical source distribution.

The total budgets for runs with emissions centred at 1500m, 2500m, and 3500m above the surface (Runs B, D, and E respectively; their horizontal locations are the same) are very similar. As the main cloud/precipitation band is several kilometres deep, similar amounts of pollutants are removed. Material at high levels is subject to more rapid advection and hence may be washed-out and deposited at different horizontal locations. Low-level sources are more affected by boundary layer diffusion, which gives rise to dry deposition. In Run C, for example, 3% of the plume is removed by this process, whereas, in runs B, D and E, dry deposition is negligible.

(b) The effect of the precipitation distribution on washout patterns: Runs F and G.

The distribution of precipitation in the warm sector band contains much small-scale variation as it passes over the UK, due to orographic influences, and also local frontogenesis, as described in section 3. To observe possible effects of this on washout and deposition the source is centred at (x, y, η) = (780, 380, 1)km, downstream of the British Isles land mass. Initially the warm front is over the source location, and the plume grows along it as the front progresses northwards. The plume at source level for Run F at 2100 GMT is shown in Fig. 10(a), with peak activity 85.4 Bqm^{-3}. Some material has risen (up to 3.9 Bqm^{-3} at 3km by this time) in the ascent to the rear of the warm front, leaving a gap at the source level. As the frontal system tracks eastwards, the plume is swept around clockwise. Material spreads vertically, advected (there is no diffusion) up- and downwards, so that at 1km the plume appears shorter at 0300 GMT (Fig. 10(b)).

Including diffusion and removal (Run G), the location of the plume material remaining airborne is as for Run F. Up to 1800h, however, there is a significant amount of deposition near and to the north west of the source (Fig. 11(a)), of material washed out by the warm-frontal precipitation. In the next 3 hours, the maximum deposited is from the northern part of the plume (Fig. 11(b)), through which passes the northern portion of the split precipitation band. The frontal uplift associated with the local frontogenesis raises the plume, but this effect is secondary to the washout incurred. Between 2100 GMT and midnight, the plume passes between the two rainband sections, and removal is less rapid then (Fig. 11(c)). That is, the peak deposition and the fraction of the plume removed are less in this interval than in neighbouring 3-hour periods. Later, as the precipitation band becomes more uniform, the cold

front approaches the source region and the plume is almost wholly aligned along it, giving the most rapid removal between midnight and 0300 GMT (Fig. 11(d)). Between 0300 and 0600 GMT, removal diminishes, as the main precipitation band has passed through the plume. The peak values in Fig. 11 are 25.8, 19.2, 14.2 and 31.1 $kBqm^{-2}$ respectively.

5. DISCUSSION.

This study is concerned with the effects of a particular frontal system, which passed over the British Isles, on some hypothetical pollutant releases. The meteorology is described by an operational model, which simulates realistically the high resolution wind, diffusion and precipitation fields necessary for the accurate prediction of contaminant dispersion and removal. Whilst these results are not validated against measurements of airborne or deposited radionuclides, they may be compared with other studies and confidence gained in their realism. This is discussed later.

Although only one meteorological case is considered, there are certain features of the frontal system which have an important bearing on the fate of contaminants, and which may be regarded as typical. These include abrupt changes in horizontal wind direction, and also cloud bands, precipitation bands and vertical motion influenced by the orography. Another feature is ascent associated with frontogenesis, leading to condensation and precipitation, latent heat release and vertical mixing. The sequence of events associated with the frontal passage is revealed by inspection of the meteorological data to be quite complex. This leads to a similar complexity in the pollutant dispersion, and plausible dynamical or physical explanations of the outcomes for different pollutant releases require the examination of data which are not routinely output from the

operational model, for instance precipitation rates aloft and diffusion coefficients. Also, derived quantities such as equivalent potential temperature and frontogenetic forcing are useful in explaining the presence of those meteorological features which directly affect dispersion and removal.

Some characteristics of the cases described in Section 4 are worthy of note, as they are likely to arise in other instances of disturbed weather conditions acting on contaminant plumes. Firstly, there are the effects of orography on the passing rainband, in that enhanced deposition can occur in mountainous regions. In comparison with the total deposition this amount may be small, but it can be significant when viewed on a local scale. As air rises over a hill range, it cools and its vapour condenses, and the earliest precipitation - that which washes out much of the pollutants if removal rates are high - is, on the mesoscale, on the upwind side of the orography. The results of Dore *et al.* (1990) for complex topography show enhancements of precipitation rate and surface deposition, a few kilometres downwind of the first peaks which the seeder cloud encounters, which may still be upwind of the main mountain range. This is not inconsistent with the results presented in section 4, since the model resolution here is somewhat coarser.

Secondly, there are the effects of the vertical velocity fields associated with fronts on the contaminant distribution. In settled conditions, vertical velocities may be small, but in "disturbed" conditions, such as those near to fronts, more rapid ascent and descent occur with vertical velocities tens of cms^{-1}. Pollutants are seen to rise several kilometres in the ascent region ahead of the cold front, and sink almost to the surface in the descent behind it (Run A). Similarly, in the vicinity of the warm front there are regions of ascent and descent close together, produced by local forcing, spreading the plume in both vertical

directions in a relatively short time (less than 3 hours in Run F). This is again complicated by orographic effects. Thirdly, the ascent regions coincide with the cloud/precipitation band, and hence there is competition between lofting and removal. For the cases described, removal dominates, but this need not be the case if less hygroscopic pollutants are considered. These, if carried high enough at first may travel further, contaminating regions far from their source. In the ascent regions, there is vertical mixing of the plume, and this turbulent mixing of the pollutants downwards may, in some locations, be more rapid than upward advection.

It is evident from the results presented here that this study demonstrates similar phenomena to those observed and modelled by others. Moreover, in some cases there are interesting contrasts in the scales at which the phenomena occur. It is observed that plumes are distorted so that they lie along fronts (see Puhakka *et al.*, 1990, in the case of the Chernobyl plume). This is due to horizontal deformation in the synoptic velocity field and to the frontal jet and conveyor belt structure. In this study, there is some diversion of plume material along the front, but this is not so marked as in the observations over mainland Europe. In that case, the fronts were not propagating as rapidly as those in this study. Also, Puhakka *et al.* (1990) noted that most of the Chernobyl fallout to the surface was due to wet deposition. Here, dry deposition only accounts for, at most, 3% of the total removal, and accordingly no results for it have been shown.

McNider *et al.* (1988) deduced that modelling the forcing of atmospheric flow on mesoscale timescales (1 to 48 hours) was necessary to simulate realistic horizontal plume spread, as turbulent mixing alone did not produce enough. The diurnal forcing produced horizontal temperature gradients and hence vertical shear of the wind. This lead to turbulent

mixing, dispersing the plume to hitherto unaffected areas. In the present study, a similar process occurs on a smaller spatial and temporal scale - that of an individual front - and the resulting lateral dispersion is similar, as it actually arises through vertical mixing. Segal *et al.* (1988), studying pollutant releases over the Florida peninsula showed a dramatic vertical spread of plumes during the day, when the planetary boundary layer was less stable, in contrast to stable nocturnal conditions. In this paper, the cloud band is associated with a deep turbulent layer (up to the tropopause) in which contaminants are mixed vertically, day or night. These two examples show that some of the effects of diurnal forcing may occur on shorter timescales when conditions are disturbed by the presence of a frontal system. The nature of the forcing may vary, but its effect on the pollutant distribution is qualitatively similar. It is more dramatic in the "frontal" case than in the "diurnal" cases, because the mixing of the plume occurs more rapidly.

The main findings of this work may be summarized as follows:

- A detailed description of the effects of travelling frontal systems on air pollution requires a high resolution (mesoscale) meteorological model in addition to the dispersion model.
- Turbulent mixing is important in the frontal cloud band through the depth of the troposphere, and therefore must be well represented in the model.
- The presence of the frontal system gives rise to horizontal and vertical diffusion of contaminants which occur more rapidly than in its absence.
- Orography is also important, through its effects on precipitation rates, and hence scavenging rates.

With regard to the last point, as individual slopes are not resolved here, there is likely to be in reality much small scale variation in the wet deposition, not captured by the model. This is true even in the

absence of orography.

There are some extensions that can be made to the modelling approach adopted in this paper, regarding the mesoscale model's ability to realistically predict the effects of meteorological phenomena on pollutant dispersion. These are, notably, effects on the initial evolution of a plume on scales smaller than the mesoscale model grid, the transport of contaminants in convective clouds which are also sub-gridscale, and the microphysical processes associated with in-cloud and below-cloud capture of contaminant particles which subsequently may be deposited. Also important is the need to verify model predictions with observations. Work on these aspects is in progress.

ACKNOWLEDGEMENTS

This study was carried out as part of the Radiological Protection Research Programme of the UK Atomic Energy Authority, with funding from the Department of Energy. The work has benefited from many useful discussions with Dr. C.E. Johnson of Harwell Laboratory and Prof. A.J. Thorpe of the Department of Meteorology, Reading University. Thanks are due also to the UK Met. Office Short Range Forecasting Research branch for providing the mesoscale model code and forecast initialization data, and to the referees for their thorough reviews of the initial drafts.

References.

Albergel A., Martin D., Strauss B. and Gros J.-M. 1988 The Chernobyl accident: modelling of dispersion over Europe of the radioactive plume and comparison with air activity measurements. *Atmos. Environ.*, **22**, 2431-2444.

Alheit R., Flossman A.I. and Pruppacher H.R. 1990 A theoretical study of the wet removal of atmospheric pollutants. IV: The uptake and redistribution of aerosol particles through the nucleation and impaction scavenging by growing cloud drops and ice particles. *J. Atmos. Sci.*, **47**, 870-887.

ApSimon H.M. and Wilson J.J.N. 1987 Modelling atmospheric dispersal of the Chernobyl release across Europe. *Boundary-Layer Meteorol.*, **41**, 123-133.

Berkowitz C.M., Easter R.C. and Scott B.C. 1989 Theory and results from a quasi-steady-state precipitation-scavenging model. *Atmos. Environ.*, **23**, 1555-1571.

Bonelli P., Calori G. and Finzi G. 1992 A fast long-range transport model for operational use in episode simulation. Application to the Chernobyl accident. *Atmos. Environ.*, **26A**, 2523-2535.

Brost R.A., Haagenson P.L. and Kuo Y.-H. 1988a The effect of diffusion on tracer puffs simulated by a regional-scale Eulerian model. *J. Geophys. Res.*, **93**, 2389-2404.

Brost R.A., Haagenson P.L. and Kuo Y.-H. 1988b Eulerian simulation of tracer distribution during CAPTEX. *J. Appl. Meteorol.*, **27**, 579-593.

Brusasca G., Tinarelli G. and Anfossi D. 1989 Comparison between the results of a Monte Carlo atmospheric diffusion model and tracer experiments. *Atmos. Environ.*, **23**, 1263-1280.

Carhart R.A., Policastro A.J., Wastag M. and Coke L. 1989 Evaluation of eight short-term long-range transport models using field data. *Atmos. Environ.*, **23**, 85-105.

Chaumerliac N., Richard E. and Rosset R. 1990 Mesoscale modeling of acidity production in orographic clouds and rain. *Atmos. Environ.*, **24A**, 1573-1584.

Dore A.J., Choularton T.W., Fowler D. and Storton-West R. 1990 Field measurements of wet deposition in an extended region of complex topography. *Q. J. R. Meteorol. Soc.*, **116**, 1193-1212.

Draxler R.R. 1987 Sensitivity of a trajectory model to the spatial and temporal resolution of the meteorological data during CAPTEX. *J. Clim. Appl. Meteorol.*, **26**, 1577-1588.

Flossman A.I. and Pruppacher H.R. 1988 A theoretical study of the wet removal of atmospheric pollutants. III: The uptake, redistribution, and deposition of $(NH_4)_2SO_4$ particles by a convective cloud using a two dimensional cloud dynamics model. *J. Atmos. Sci.*, **45**, 1857-1871.

Flossman A.I. 1991 The scavenging of two different types of marine aerosol particles calculated using a two-dimensional detailed cloud model. *Tellus*, **43B**, 301-321.

Golding B.W. 1990 The Meteorological Office mesoscale model. *Meteorological Magazine*, **119**, 81-96.

Gryning S.-E. 1985 The Øresund experiment - a Nordic mesoscale dispersion experiment over a land-water-land area. *Bulletin of the American Meteorological Society*, **66**, 1403-1407.

Hass H., Memmesheimer M., Geiss H., Jakobs H.J., Laube M. and Ebel A. 1990 Simulation of the Chernobyl radioactive cloud over Europe using the EURAD model. *Atmos. Environ.*, **24A**, 673-692.

Hegg D.A., Rutledge S.A. and Hobbs P.V. 1984 A numerical model for sulfur chemistry in warm frontal rainbands. *J. Geophys. Res.*, **89**, 7133-7147.

Hegg D.A., Rutledge S.A. and Hobbs P.V. 1986 A numerical model for sulfur and nitrogen scavenging in narrow cold-frontal rainbands. II: Discussion of chemical fields. *J. Geophys. Res.*, **91**, 14404-14416.

Hill T.A., Jones A. and Choularton T.W. 1987 Modelling sulphate deposition onto hills by washout and turbulence. *Q. J. R. Meteorol. Soc.*, **113**, 1217-1236.

Jylhä K. 1991 Empirical scavenging coefficients of radioactive substances released from Chernobyl. *Atmos. Environ.*, **25A**, 263-270.

Kao C.-Y. and Yamada T. 1988 Use of the CAPTEX data for evaluations of a long-range transport numerical model with a four-dimensional data assimilation technique. *Mon. Weather Rev.*, **116**, 293-306.

Ku J.-Y., Rao S.T. and Rao K.S. 1987 Numerical simulation of air pollution in urban areas. *Atmos. Environ.*, **21**, 201-212.

Kuo Y.-H., Skumanich M., Haagenson P.L. and Chang J.S. 1985 The accuracy of trajectory models as revealed by the observing system simulation experiments. *Mon. Weather Rev.*, **113**, 1852-1867.

Maryon R.H. 1989 Trajectory and plume analysis in the Meteorological Office Atmospheric Dispersion Group. *Meteorological Magazine*, **118**, 117-127.

McNider R.T., Moran M.D. and Pielke R.A. 1988 Influence of diurnal and inertial boundary-layer oscillations on long-range dispersion. *Atmos. Environ.*, **22**, 2445-2462.

Nickerson E.C., Richard E., Rosset R. and Smith D.R. 1986 The numerical simulation of clouds, rain and airflow over the Vosges and Black Forest mountains: A meso-β model with parameterized microphysics. *Mon. Weather Rev.*, **114**, 398-414.

Piedelievre J.P., Musson-Genon L. and Bompay F. 1990 MEDIA - An Eulerian model of atmospheric dispersion: first validation on the Chernobyl release. *J. Appl. Meteorol.*, **29**, 1205-1220.

Puhakka T., Jylhä K., Saarikivi P. and Koistinen J. 1990 Meteorological factors affecting the radioactive deposition in Finland after the Chernobyl accident. *J. Appl. Meteorol.*, 29, 813-829.

Rutledge S.A., Hegg D.A. and Hobbs P.V. 1986 A numerical model for sulfur and nitrogen scavenging in narrow cold-frontal rainbands. I: Model description and discussion of microphysical fields. *J. Geophys. Res.*, 91, 14385-14402.

Rutledge S.A. and Hobbs P.V. 1983 The mesoscale and microscale structure and organization of clouds and precipitation in midlatitude cyclones. VIII: A model for the "seeder-feeder" process in warm-frontal rainbands. *J. Atmos. Sci.*, 40, 1185-1206.

Saylor R.D., Peters L.K. and Mathur R. 1991 The STEM-II regional-scale acid deposition and photochemical oxidant model. III. A study of mesoscale acid deposition in the Lower Ohio River valley. *Atmos. Environ.*, 25A, 2873-2894.

Scott B.C. 1982 Theoretical estimates of the scavenging coefficient for soluble aerosol particles as a function of precipitation type, rate and altitude. *Atmos. Environ.*, 26, 1753-1762.

Segal M., Pielke R.A., Arritt R.W., Moran M.D., Yu C.-H. and Henderson D. 1988 Application of a mesoscale atmospheric dispersion modeling system to the estimation of SO_2 concentrations from major elevated sources in southern Florida. *Atmos. Environ.*, 22, 1319-1334.

Slinn W.G.N. 1979 Some approximations for the wet and dry removal of particles and gases from the atmosphere. *Water, Air and Soil Pollution*, 7, 513-543.

Slinn W.G.N. 1984 Precipitation scavenging. In, Atmospheric Science and Power Production. ed. Randerson. U.S. Dept. of Energy.

Sweby P.K. 1984 High resolution schemes using flux limiters for hyperbolic conservation laws. *SIAM Journal of Numerical Analysis*, 21, 995-1011.

Tapp M.C. and White P.W. 1976 A non-hydrostatic mesoscale model. *Q. J. R. Meteorol. Soc.*, 102, 277-296.

Tsai W. 1987 A wet removal study of air pollutants using a one-dimensional transport/transformation/removal model. Ph.D. Dissertation, Rensselaer Polytechnic Institute.

Wright B.J. and Golding B.W. 1990 The interactive mesoscale initialization. *Meteorological Magazine*, 119, 234-244.

Yamada T. and Mellor G.L. 1979 A numerical simulation of BOMEX data using a turbulence closure model coupled with ensemble cloud relations. *Q. J. R. Meteorol. Soc.*, 105, 915-944.

Yoshikawa T., Kimura F., Koide T. and Kurita S. 1990 An emergency computation model for the wind field and diffusion during accidental nuclear pollutants releases. *Atmos. Environ.*, 24A, 2739-2748.

Figures.

1) Surface pressure analysis for 1800 GMT 4 March 1991.

2) Mesoscale model results at 1500 GMT 4 March 1991: equivalent potential temperature (K) (thick solid lines), precipitation rate (shaded: light > 1 mm h^{-1}, medium > 3 mm h^{-1}, dark > 5 mm h^{-1}), horizontal velocity (vectors). (a) z = 3500m, (b) z = 1500m, (c) z = 500m. Max. speeds are 32.7, 31.3 and 30.9 ms^{-1}, respectively.

3) As Fig. 2, but for 2100 GMT. Maximum speeds are 31.1, 33.1 and 31.2 ms^{-1} respectively.

4) As Fig. 2, but for 0300 GMT 5 March 1991. Maximum speeds are 28.4, 27.2 and 29.1 ms^{-1} respectively.

5) Run A contaminant at z = 1.5km. (a) 1800 GMT 4 March 1991, (b) midnight and (c) 0600 GMT 5 March 1991. Contour interval is 10 Bqm^{-3}.

6) Run A for 1800 GMT 4 March 1991. (a) Contaminant at z = 3.5km. Contour interval is 4 Bqm^{-3}, maximum value is 18.8 Bqm^{-3}. The source location is marked with a cross. (b) x-integrated contaminant in yz-plane, axes in km, contours every 400 $kBqm^{-2}$ to 2000 $kBqm^{-2}$. The maximum value is 3600 $kBqm^{-2}$. The horizontal axis runs south to north and the line z = 3.5 is plotted for comparison with part (a).

7) Contaminant at z = 500m (Bqm^{-3}). (a) Run A, 0600 GMT and (b) run B, 2100 GMT 4 March 1991. (c) Run B 0300 GMT and (d) run B 0600 GMT 5 March 1991. Contour interval is 2 Bqm^{-3}. The peak value is 12.0 Bqm^{-3} in (c).

8) Wet deposition ($kBqm^{-2}$). (a) Run B 1200 to 2100 GMT 4 March 1991; (b) run B midnight to 0600 GMT 5 March 1991; (c) run C, 1200 to 2100 GMT 4 March 1991 and (d) run C, midnight to 0600 GMT 5 March 1991. Contours are from 5 $kBqm^{-2}$ to 30 $kBqm^{-2}$, at intervals of 5 $kBqm^{-2}$. Maxima are 78.9 and 77.5 in (a) and (c), respectively.

9) Volume integrated activity. Run B: airborne total (solid line) and deposited amount (dotted line). Run C: airborne total (dashed line) and deposited (dot-dashed).

10) Run F contaminant at z = 1 km (Bqm^{-3}). (a) 2100 GMT 4 March 1991 and (b) 0300 GMT 5 March 1991. Contour interval is 20 Bqm^{-3}, with maxima approximately 85 Bqm^{-3}. The source is located at the southern end of the plume.

11) Run G wet deposition ($kBqm^{-2}$). (a) 1200 to 1800 GMT, (b) 1800 to 2100 GMT, (c) 2100 to midnight GMT 4 March 1991, (d) midnight to 0300 GMT 5 March 1991. Contour interval is 5 $kBqm^{-2}$. See text for maximum values.

Table 1. Source location for the idealised releases.

Run	Source centre location.			Vertical diffusion
	x (km)	y (km)	η (m)	and wet deposition.
A	400	150	1500	No.
B	400	150	1500	Yes.
C	400	150	500	Yes.
D	400	150	2500	Yes.
E	400	150	3500	Yes.
F	780	380	1000	No.
G	780	380	1000	Yes.

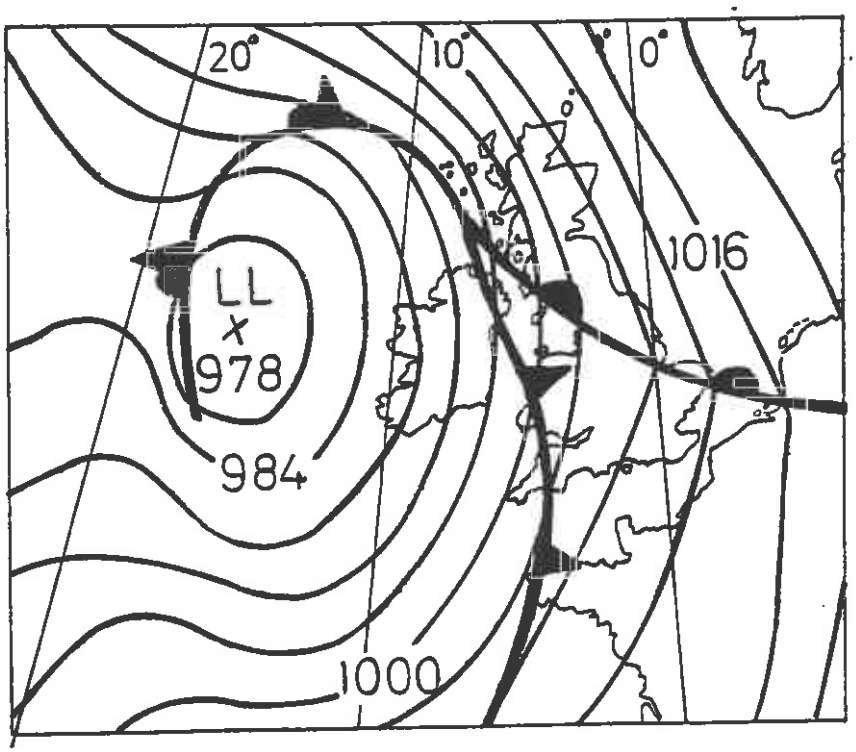

Figure 1: Surface pressure analysis for 1800h on 4 March, 1991.

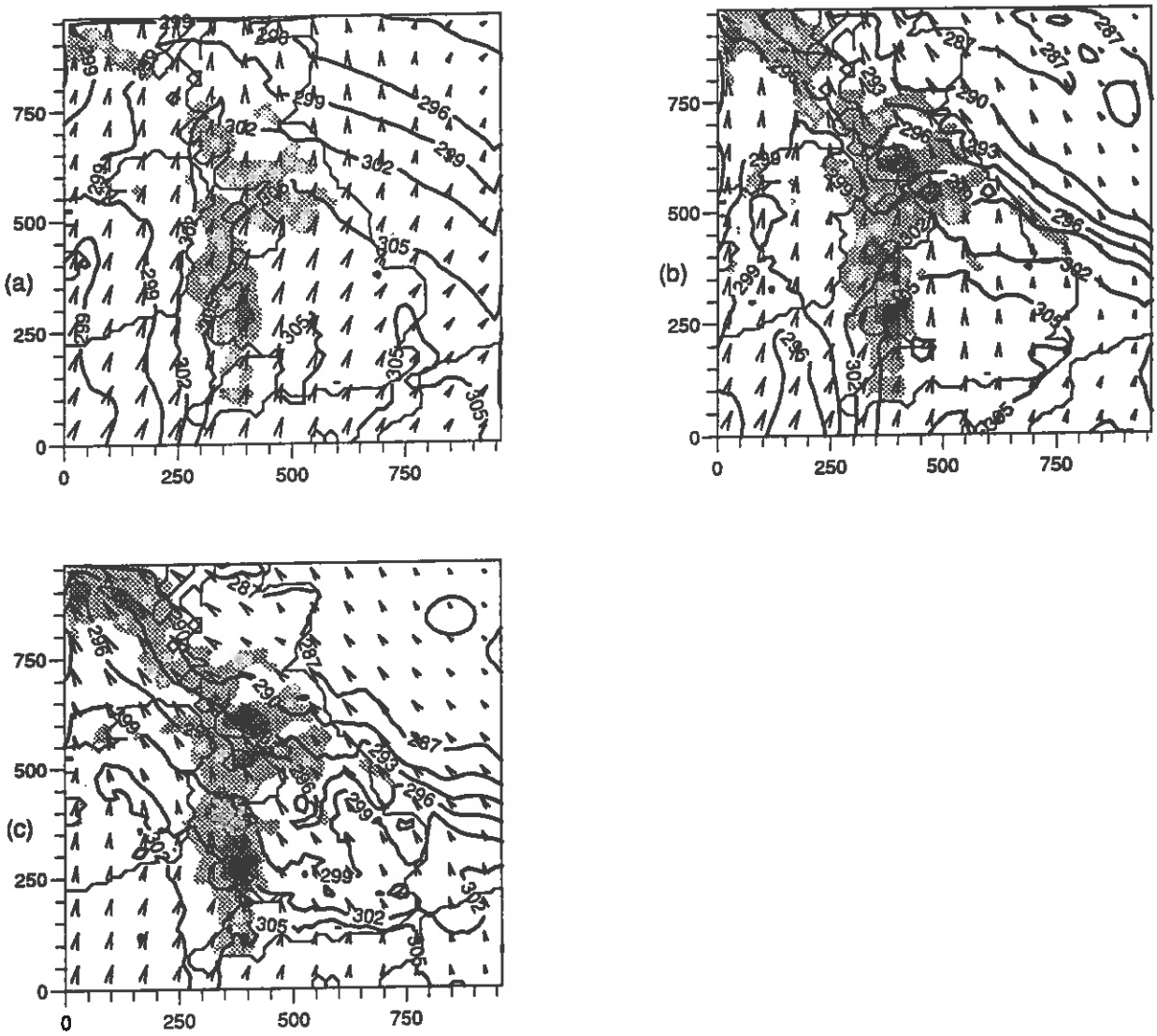

Figure 2: Mesoscale model results at 1500h: equivalent potential temperature (thick solid lines, in Kelvins), precipitation rate (shaded, light greater than 1 mm/h, medium greater than 3 mm/h, dark greater than 5 mm/h), horizontal velocity (vectors). (a) z = 3500m , (b) z = 1500m, (c) z = 500m. Max. speeds are 32.7, 31.3 and 30.9 m/s, resp.

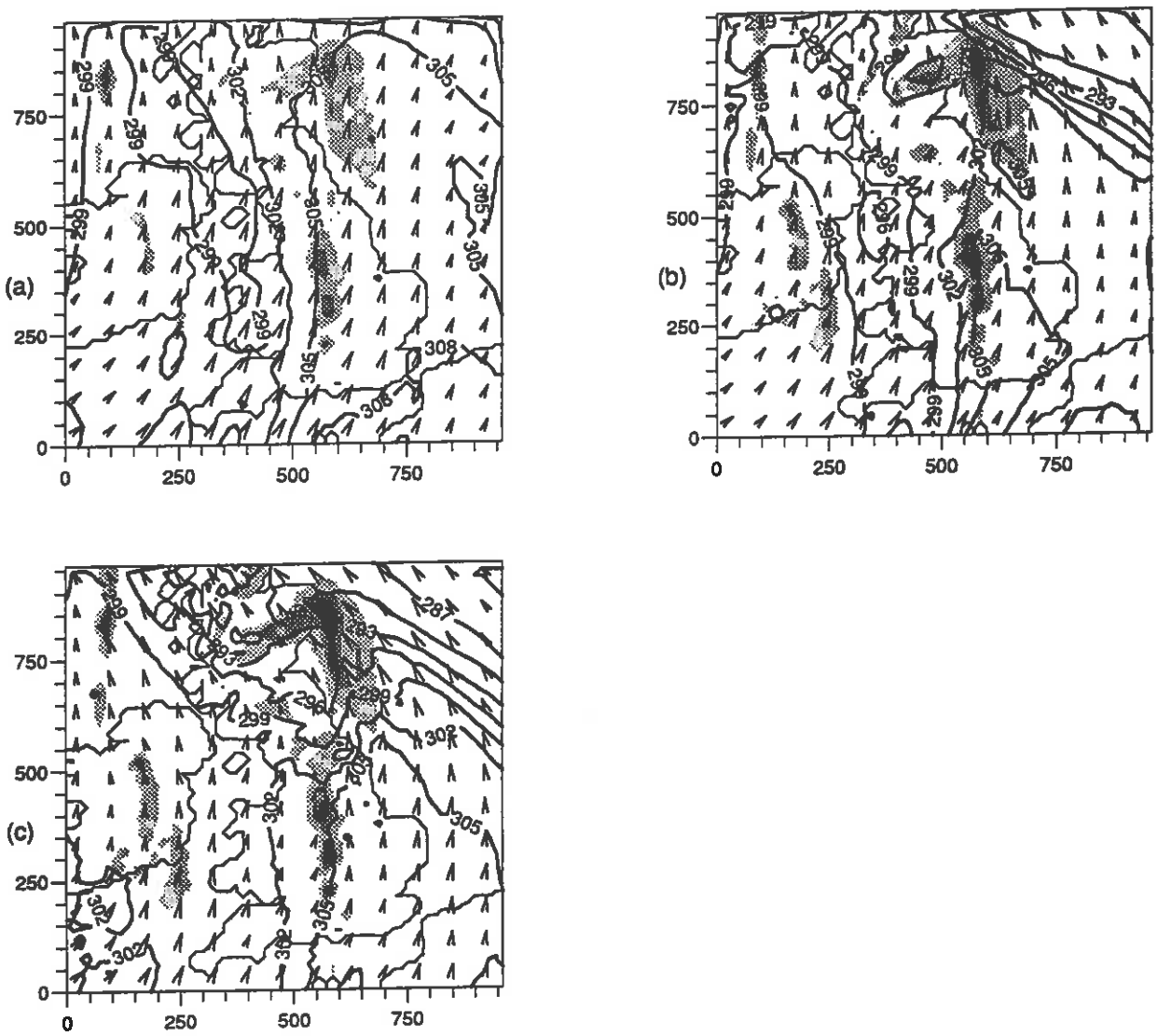

Figure 3: As Figure 2, but for 2100h. Max. speeds are 31.1, 33.1 and 31.2 m/s respectively.

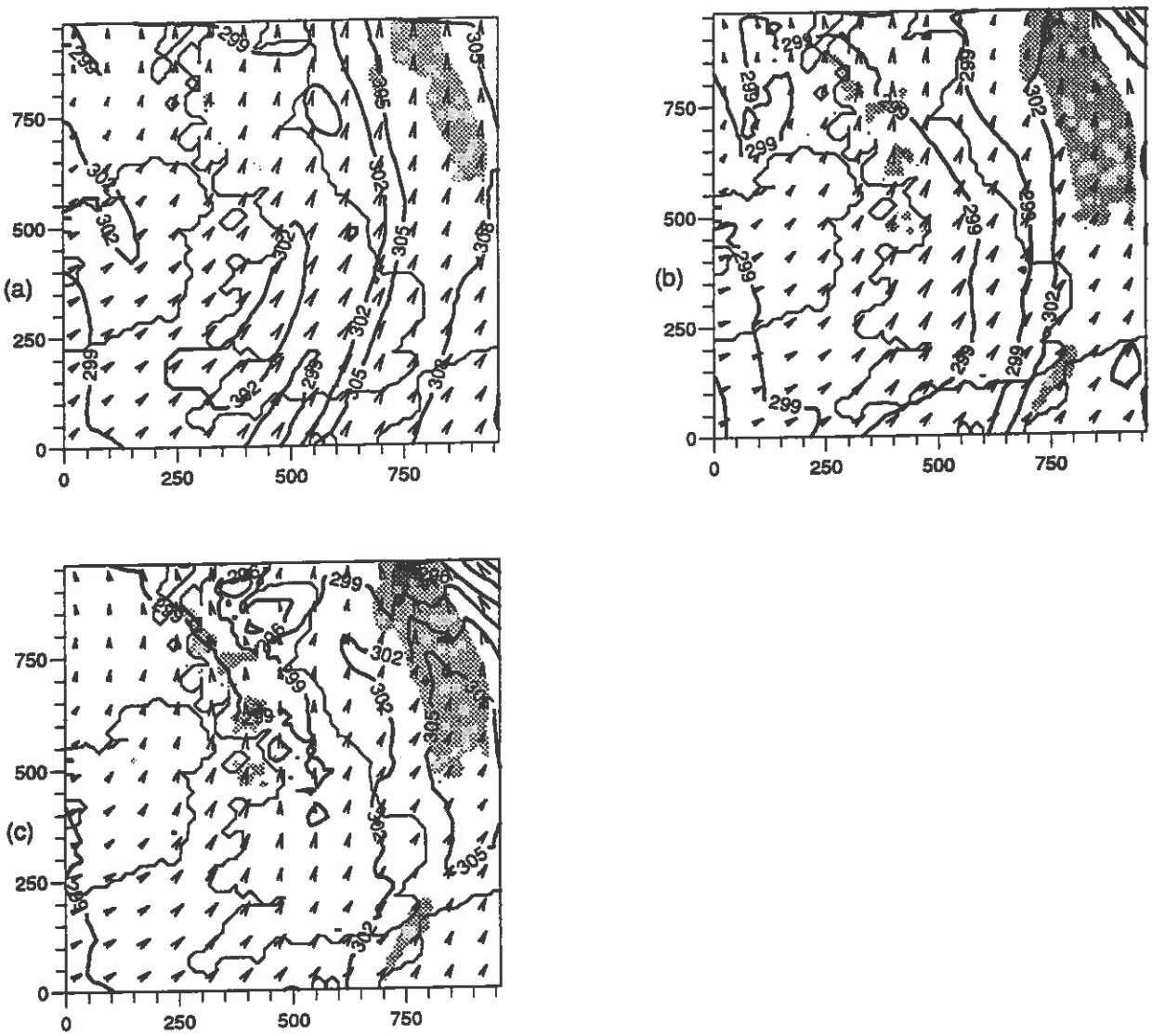

Figure 4: As Figure 2, but for 0300h. Max. speeds are 28.4, 27.2 and 29.1 m/s respectively.

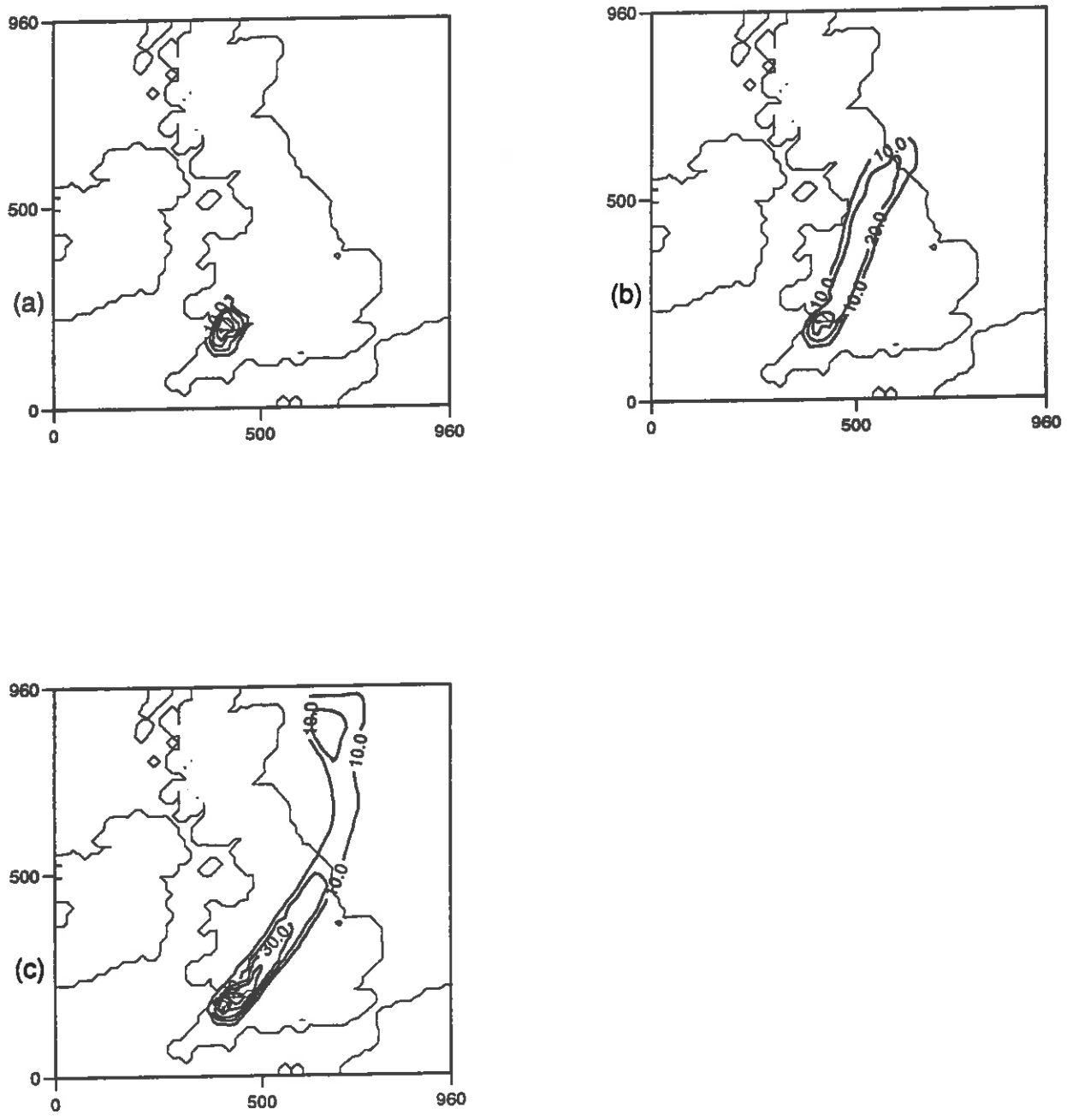

Figure 5: Run A, contaminant at 1.5km.
a) 1800h, b) midnight c) 0600h.
Contour interval 10 Bq/m3.

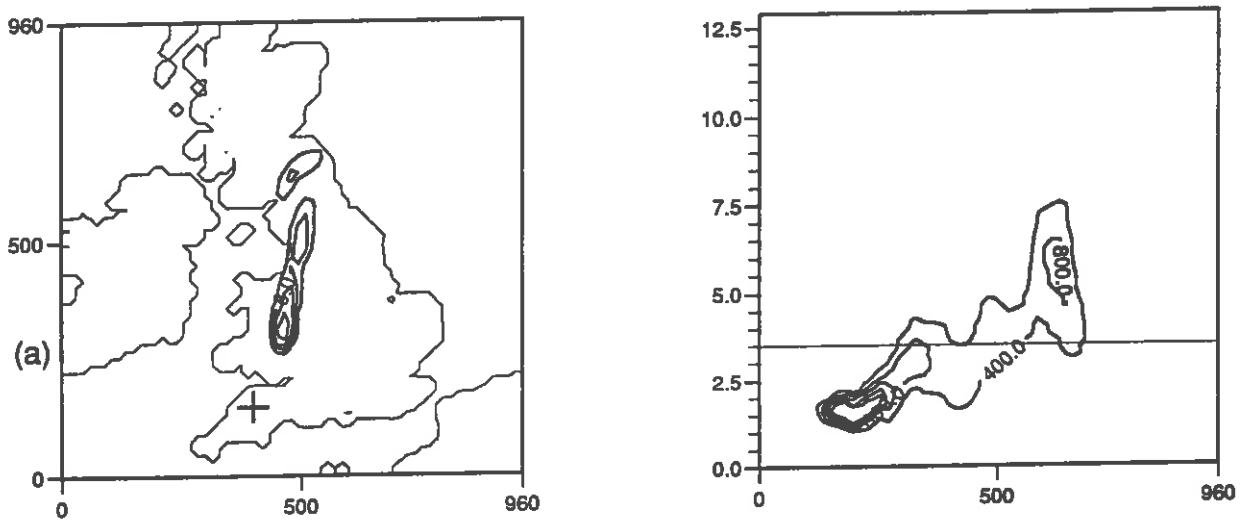

Figure 6: Run A, 1800h. a) Contaminant at 3.5km. Contour interval 4 Bq/m3, maximum value 18.8 Bq/m3. The source location is marked with a cross. b) x-integrated contaminant in yz-plane, axes in km, contours in 400 kBq/m2 intervals, to 2000 kBq/m2. The maximum value is 3600 kBq/m2. The horizontal axis runs south to north and the line z = 3.5 km is plotted for comparison with part (a).

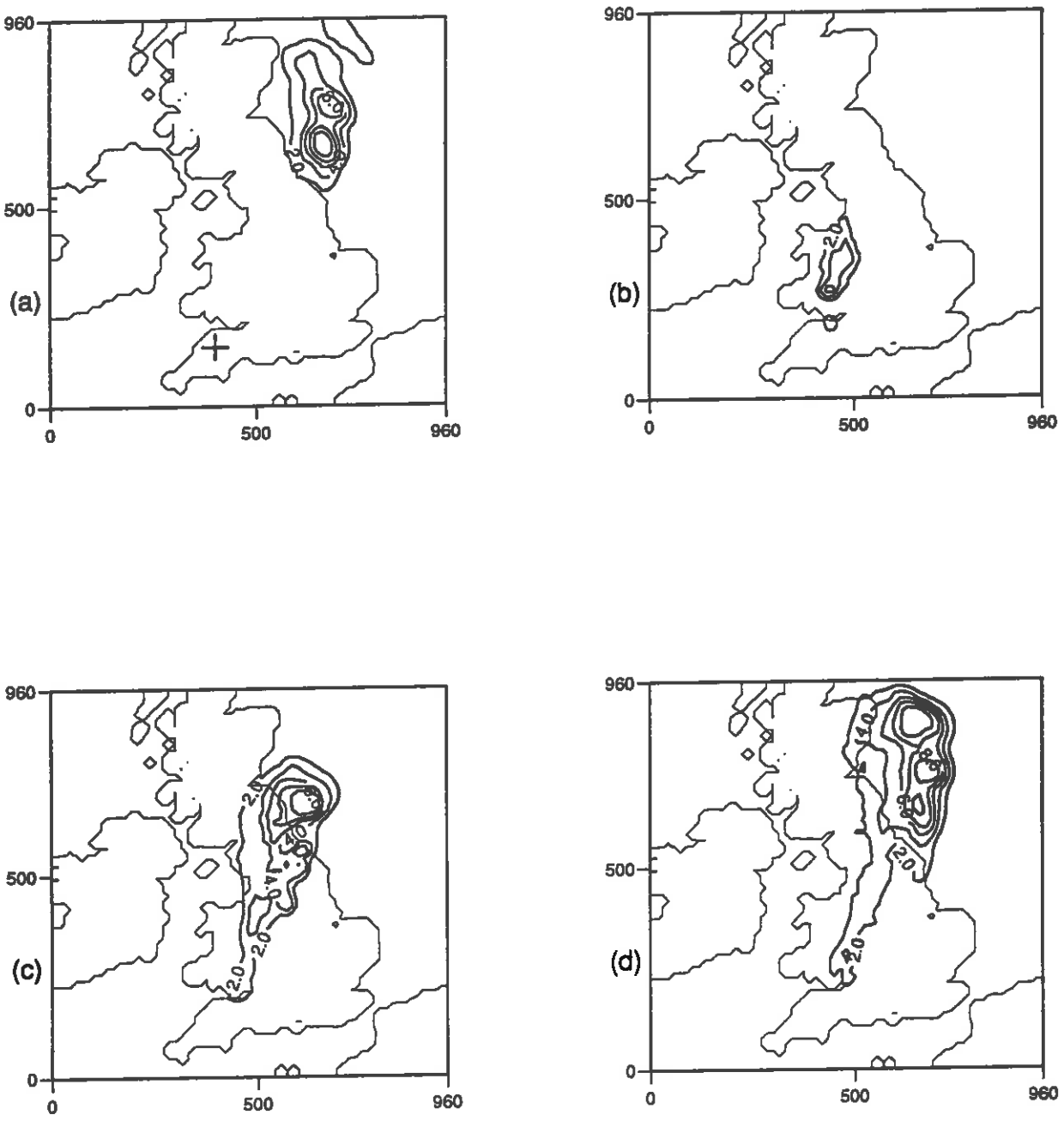

Figure 7: Contaminant at z = 500m, in Bq/m3.
a) Run A, 0600h, b) Run B, 2100h, c) Run B 0300h,
d) Run B 0600h. Contour interval 2 Bq/m3. The peak
value is 12.0 Bq/m3, in (c).

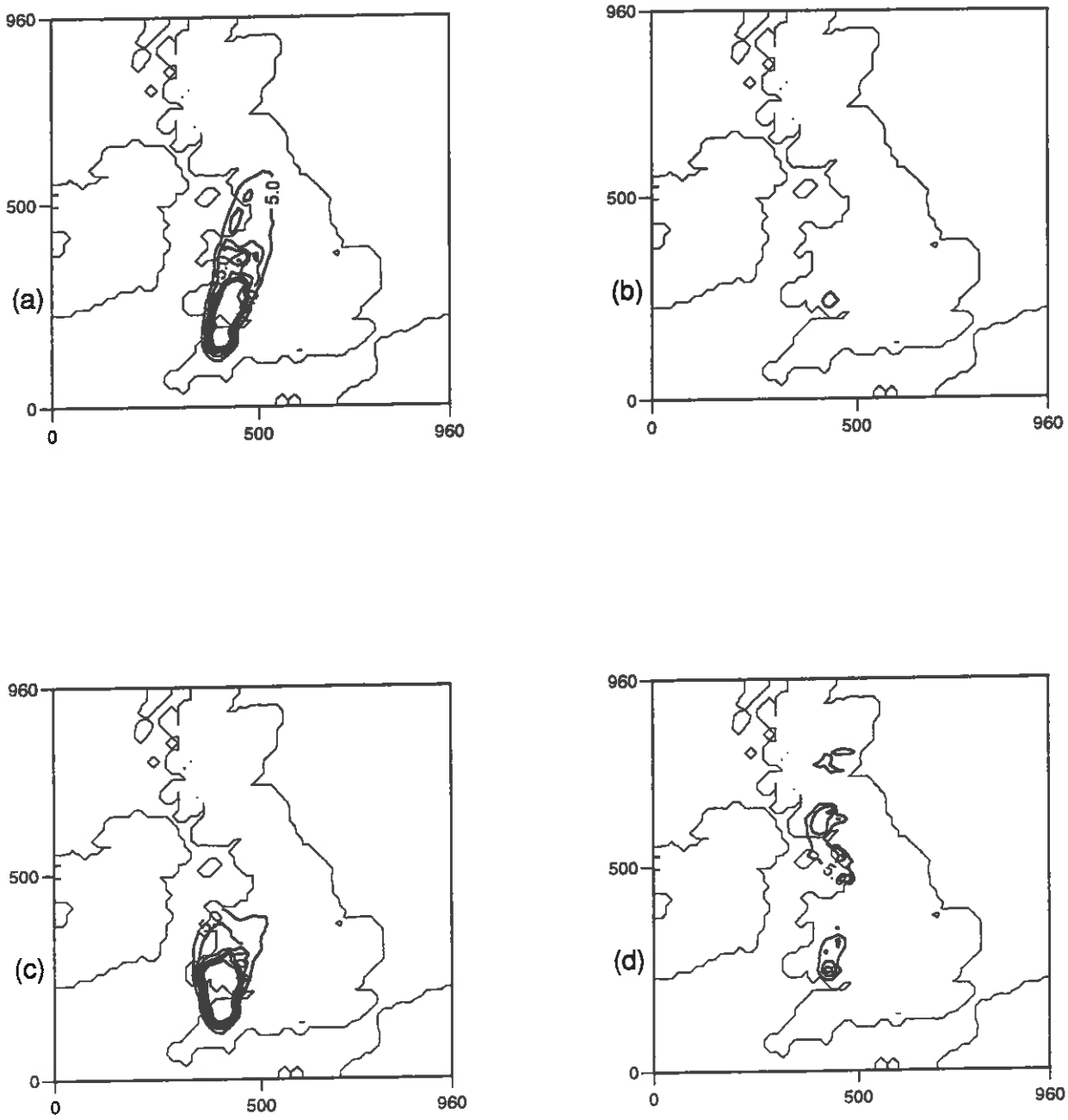

Figure 8: Wet deposition, in kBq/m2. a) Run B, 1200h to 2100h, b) Run B, midnight to 0600h, c) Run C, 1200h to 2100h, d) Run C, midnight to 0600h. Contours are from 5 kBq/m2 to 30 kBq/m2, at intervals of 5 kBq/m2. Maxima are 78.9 and 77.5 in (a) and (c), respectively.

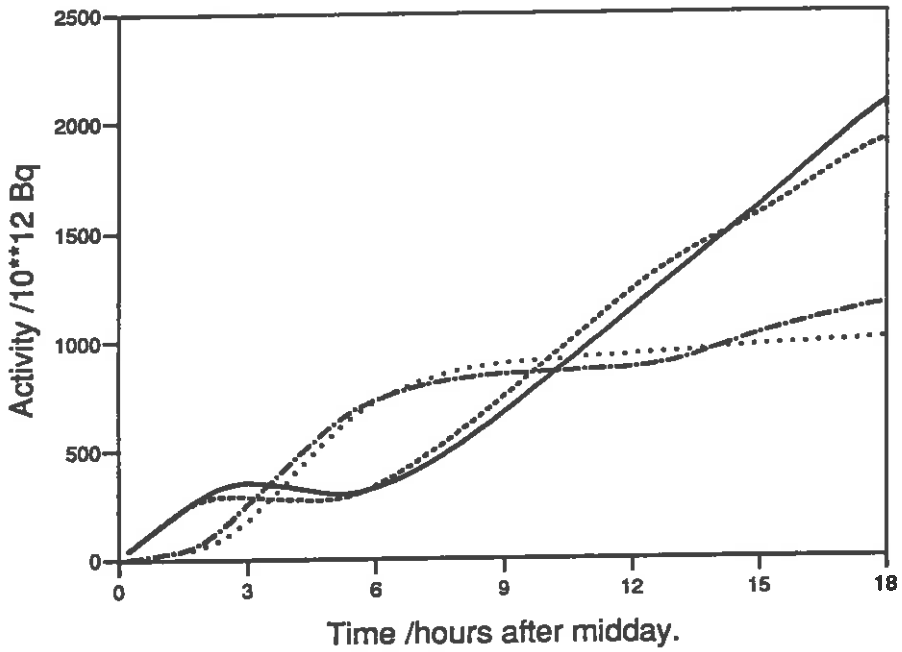

Fig. 9: Volume integrated activity. Run B: airborne total (solid line) and deposited amount (dotted line). Run C: airborne total (dashed line) and deposited (dot-dashed).

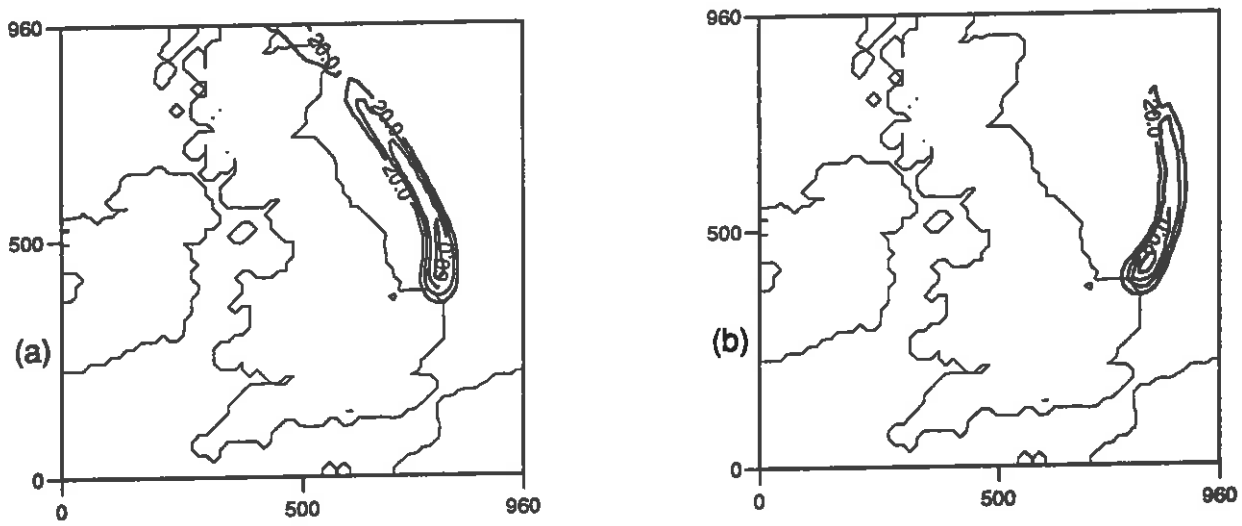

Figure 10: Run F, contaminant at 1 km, in Bq/m3. a) 2100h, b) 0300h.
Contour interval is 20 Bq/m3, with maxima approximately 85 Bq/m3.
The source is located at the southern end of the plume.

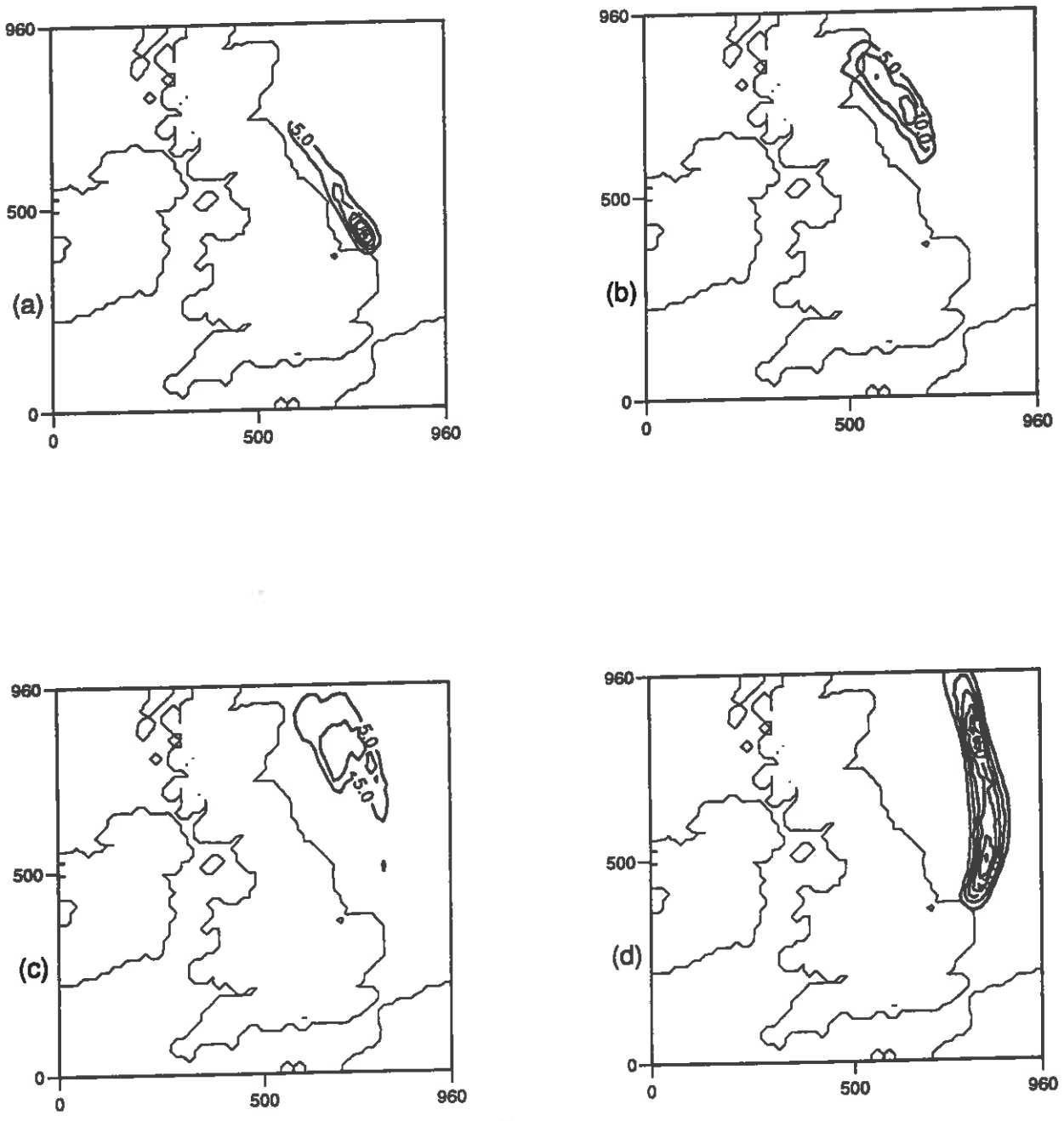

Figure 11: Run G, wet deposition in kBq/m2. a) 1200h to 1800h, b) 1800h to 2100h, c) 2100h to midnight, d) midnight to 0300h. Contour interval is 5 kBq/m2. See text for maximum values.

CURRENT JCMM INTERNAL REPORTS

This series of JCMM Internal Reports, initiated in 1993, contains unpublished reports and also versions of articles submitted for publication. The complete set of Internal Reports is available from the National Meteorology Library on loan, if required.

1. **Research Strategy and Programme.**
   K A Browning et al
   January 1993

2. **The GEWEX Cloud System Study (GCSS).**
   GEWEX Cloud System Science Team
   January 1993

3. **Evolution of a mesoscale upper tropospheric vorticity maximum and comma cloud from a cloud-free two-dimensional potential vorticity anomaly.**
   K A Browning
   January 1993

4. **The Global Energy and Water Cycle**
   K A Browning
   July 1993

5. **Structure of a midlatitude cyclone before occlusion.**
   K A Browning and N Roberts
   July 1993

6. **Developments in Systems and Tools for Weather Forecasting.**
   K A Browning and G Szejwach
   July 1993

7. **Diagnostic study of a narrow cold frontal rainband and severe winds associated with a stratospheric intrusion.**
   K A Browning and R Reynolds
   August 1993

8. **Survey of perceived priority issues in the parametrizations of cloud-related processes in GCMs.**
   K A Browning
   September 1993

9. **The Effect of Rain on Longwave Radiation.**
   I Dharssi
   September 1993

10. **Cloud Microphysical Processes - A Description of the Parametrization used in the Large Eddy Model.**
H Swann
July 1994

11. **An Appreciation of the Meteorological Research of Ernst Kleinschmidt.**
A J Thorpe
May 1992

12. **Potential Vorticity of Flow Along the Alps.**
A J Thorpe, H Volkert and Dietrich Heimann
August 1992

13. **The Representation of Fronts.**
A J Thorpe
January 1993

14. **A Parametrization Scheme for Symmetric Instability: Tests for an Idealised Flow.**
C S Chan and A J Thorpe
February 1993

15. **The Fronts 92 Experiment: a Quicklook Atlas.**
Edited by T D Hewson
November 1993

16. **Frontal wave stability during moist deformation frontogenesis. Part 1. Linear wave dynamics**
C H Bishop and A J Thorpe
May 1993

17. **Frontal wave stability during moist deformation frontogenesis. Part 2. The suppression of non-linear wave development.**
C H Bishop and A J Thorpe
May 1993

18. **Gravity waves in sheared ducts.**
S Monserrat and A J Thorpe
October 1993

19. **Potential Vorticity and the Electrostatics Analogy: Quasi-Geostrophic Theory.**
C Bishop and A J Thorpe
November 1993

20. **Recent Advances in the Measurement of Precipitation by Radar.**
A J Illingworth
April 1993

21. **Micro-Physique et Givrage. Cloud Microphysics and Aircraft Icing.**
A J Illingworth
May 1993

22. **Differential Phase Measurements of Precipitation.**
M Blackman and A J Illingworth
May 1993

23. **Estimation of Effective Radius of Cloud Particles from the Radar Reflectivity.**
N I Fox and A J Illingworth
May 1993

24. **A Simple Method of Dopplerising a Pulsed Magnetron Radar.**
L Hua, A J Illingworth and J Eastment
November 1993

25. **Radiation and Polar Lows.**
George C Craig
February 1994

26. **Collected preprints submitted to International Symposium on the Life Cycles of Extratropical Cyclones; Bergen, Norway, 27 June - 1 July 1994**
April 1994

27. **Convective Frontogenesis**
Douglas J Parker and Alan J Thorpe
April 1994

28. **Improved Measurement Of The Ice Water Content In Cirrus Using A Total Water Evaporator**
Philip R A Brown and Peter N Francis
April 1994

29. **Mesoscale Effects of a Dry Intrusion within a Vigorous Cyclone**
K A Browning and B W Golding
April 1994

30. **GEWEX Cloud System Study, Science Plan**
May 1994

31. **Parametrization of Momentum Transport by Convectively Generated Gravity Waves**
R Kershaw
May 1994

32. **Mesoscale Modelling Newsletter, No. 5**
May 1994

33. **Observations of the mesoscale sub-structure in the cold air of a developing frontal cyclone**
K A Browning, S A Clough, C S A Davitt, N M Roberts and T D Hewson
May 1994

34. **Longwave Radiative Forcing of a Simulated Tropical Squall Line**
Imtiaz Dharssi
July 1994

35. **On the nature of the convective circulations at a kata-cold front**
K A Browning
September 1994

36. **Collected preprints of papers submitted to the COST-75 International Seminar on Advanced Weather Radar Systems, Brussels, 20-23 September 1994**
November 1994

37. **Use of satellite imagery to diagnose events leading to frontal thunderstorms: Parts I and II of a case study**
K A Browning and N M Roberts
November 1994

38. **The role of spaceborne millimetre-wave radar in the global monitoring of ice cloud**
P R A Brown, A J Illingworth, A J Heymsfield, G M McFarquhar, K A Browning and M Gosset
December 1994

39. **Potential Vorticity Inversion**
Michal Ziemianski
October 1994

40. **Theory of mature tropical cyclones; A comparison between Kleinschmidt (1951) and Emanual (1986)**
Suzanne L Gray
December 1994

41. **Dispersion and removal of pollutants during the passage of an atmospheric frontal system**
N R Gimson
December 1994

42. **The role of snow sublimation in frontogenesis**
D J Parker and A J Thorpe
December 1994

43. **Potential vorticity and the electrostatics Analogy: Ertel-Rossby formulation**
A J Thorpe and C H Bishop
December 1994

Met Office Joint Centre for Mesoscale Meteorology Department of Meteorology
University of Reading PO Box 243 Reading RG6 6BB United Kingdom
Tel: +44 (0)118 931 8425 Fax: +44 (0)118 931 8791
www.metoffice.com